

# A Demonstration of Broadband Cavity-Enhanced Absorption Spectroscopy at Deep-Ultraviolet Wavelengths: Application to Sensitive Real-Time Detection of the Aromatic Pollutants Benzene, Toluene, and Xylene

Meng Wang, Ravi Varma, Dean S. Venables, Wu Zhou, and Jun Chen\*



Cite This: *Anal. Chem.* 2022, 94, 4286–4293



Read Online

ACCESS |



Metrics & More

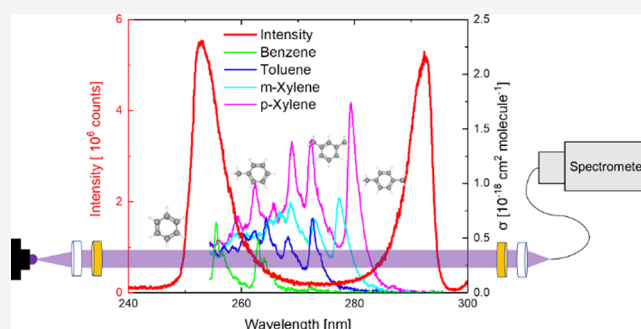


Article Recommendations



Supporting Information

**ABSTRACT:** Benzene, toluene, and xylene (BTX) are serious air pollutants emitted by the chemical industry. Real-time monitoring of these air pollutants would be a valuable tool to regulate emissions of these compounds and reduce the harm they cause to human health. Here, we demonstrate the first detection of BTX using incoherent broadband cavity-enhanced absorption spectroscopy (IBBCEAS). The instrument was operated in the deep-ultraviolet spectral region between 252 and 286 nm, where aromatic compounds have intense  $\pi \rightarrow \pi^*$  absorption bands. The mirror reflectivity was calibrated by two methods and exceeded 99.63% at 266 nm. At an integration time of 60 s, the  $1\sigma$  measurement sensitivities were estimated to be 7.2 ppbv for benzene, 21.9 ppbv for toluene, 10.2 ppbv for *m*-xylene, and 4.8 ppbv for *p*-xylene, respectively. The absorption cross sections of BTX were measured in this work with an uncertainty of 10.0% at a resolution of 0.74 nm. The absorption cross sections reported in this work were in good agreement with those from earlier studies after accounting for differences in spectral resolution. To demonstrate the ability of the instrument to quantify complex mixtures, the concentrations of *m*-xylene and *p*-xylene have been retrieved under five different mixing ratios. Instrumental improvements and measurements strategies for use in different applications are discussed.



## 1. INTRODUCTION

Benzene, toluene, and xylene (BTX) are an important class of volatile organic compounds in the atmosphere that primarily enter the atmosphere from vehicles, biomass burning, solvent use, and the petrochemical industry.<sup>1,2</sup> Benzene is a known carcinogen and increases the risk of other illnesses. It is a notorious cause of bone marrow failure. The primary reaction pathways for monocyclic aromatics are reaction with hydroxyl radicals to form phenols or degradation to carbonyls, such as glyoxal.<sup>3–5</sup> Oxidation of BTX also produces secondary organic aerosols and ozone, thereby aggravating air pollution and exacerbating impacts on public health.<sup>6,7</sup>

Analytical methods for quantifying BTX in the air usually include absorption traps and subsequent separation by gas chromatography with detection by flame ionization, photoionization, or mass chromatography.<sup>8,9</sup> Measurement time resolution is usually about 30–60 min per sample. In recent years in situ optical methods, such as long path differential optical absorption spectroscopy (LP-DOAS), have also been applied.<sup>10</sup> Unlike other methods, LP-DOAS uses a long physical path (typically 500–1000 m) and measures the path-integrated concentration over this distance. However, the

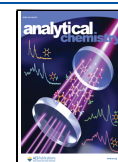
correlation between the two types of methods is poor because of the different spatial scales; DOAS usually reports higher values than in situ methods.<sup>11</sup>

Incoherent broadband cavity-enhanced absorption spectroscopy (IBBCEAS) has been applied to many gaseous molecules since it was first proposed by Fiedler et al, mostly at visible wavelengths.<sup>12</sup> There are few applications in the UV range.<sup>13–17</sup> Optical cavity measurements in the UV range are challenging for several reasons: (1) CCD detectors have relatively low quantum efficiency in the UV, and light sources are less intense in this region. (2) Losses at optical cavity mirror surfaces by scattering and absorption are much higher than at longer wavelengths. (3) System sensitivity is limited by Rayleigh scattering at short wavelengths. (4) Increasing Mie scattering from particles, and strong ozone absorption is a

**Received:** November 13, 2021

**Accepted:** February 23, 2022

**Published:** March 4, 2022



challenge for atmospheric samples. As a result of the high inherent losses in the sample gas and the lower mirror reflectivity, the extremely long effective light pathlengths attained by optical cavity instruments at visible and near-infrared wavelengths are not feasible below 300 nm. Nevertheless, the ability to measure absorption and scattering at deep-UV wavelengths with high sensitivity would be valuable for fundamental research, monitoring of ambient air quality<sup>10</sup> and industrial emissions,<sup>11</sup> and other uses.

To date, there have been few applications of optical cavity methods below 300 nm. Ityaksov and coworkers used cavity ring-down spectroscopy with a dye laser to measure Rayleigh scattering cross sections of N<sub>2</sub>, CH<sub>4</sub>, and SF<sub>6</sub> between 198 and 270 nm.<sup>18</sup> Prior work with broadband cavity instruments includes a deep-UV CEAS instrument using a mercury atomic emission lamp (254 nm) to measure gaseous mercury and ozone with detection limits of 8.1 and 8.4 ppbv, respectively, in 10 s acquisition time,<sup>19</sup> an IBBCEAS system combining a laser-driven light source (LDLS) and LED to measure acetone between 272 and 292 nm with an LOD of 8 ppmv in 1 s acquisition time,<sup>20</sup> and a deep UV-LED system at 280 nm that measured ozone with an LOD below 0.1 ppm with an accuracy of 0.5%.<sup>21</sup>

The aim of this work is to build on these prior studies and demonstrate that IBBCEAS is a useful approach for highly sensitive measurements of sample extinction at deep-UV wavelengths. We describe an LED IBBCEAS spectrometer operating in the 252–286 nm wavelength range, which achieves an LOD of  $3.7 \times 10^{-7} \text{ cm}^{-1}$  with a 60 s acquisition time, a sensitivity high enough to be valuable for studying many compounds that absorb strongly at these wavelengths. We demonstrate that this instrument can be used to make sensitive, real-time measurements of aromatic compounds, specifically the important environmental pollutants BTX, and has potential applications in laboratory research, emissions monitoring, and other combined applications.<sup>22</sup>

## 2. EXPERIMENTAL SECTION

**2.1. Instrument Setup.** The IBBCEAS approach was first described by Fiedler et al.<sup>12</sup> and has been applied in many studies.<sup>23,24</sup> In this work, the deep-UV IBBCEAS instrument comprised three subsystems: the light source, optical cavity, and detection module (Figure 1a). The light source was a 255 nm LED (HSE255H-M807X, Hasunopto, China) with an FWHM of 11 nm, and the operation status was 5.3 V forward voltage and 0.17 A current. The LED was mounted on a thermostat and driven by a constant current source to minimize current and temperature fluctuations. The thermostat was stabilized to  $15 \pm 0.1 \text{ }^\circ\text{C}$  using a PID controller.

The light emitted from the LED was collected and focused by a lens ( $f = 35 \text{ cm}$ ) into a high-finesse optical cavity formed by a pair of high-reflectivity (HR) mirrors (Layertec GmbH). The reflectivity of the HR mirror between 250 and 280 nm was specified by the manufacturer to be greater than 0.995. The cavity mirrors were separated by  $96.75 \pm 0.02 \text{ cm}$ . Light transmitted through the cavity was focused by another lens ( $f = 75 \text{ cm}$ ), filtered by a short-pass filter (Semrock FF01-300/SP-25; transmission >70% between 255 and 290 nm), and coupled into a quartz fiber bundle. The fiber bundle was 1.5 m long and consisted of  $20 \times 200 \text{ }\mu\text{m}$  core fibers (Figure 1a). The fibers were vertically arranged at the entrance slit of an imaging spectrograph to optimize light coupling and maximize the signal.

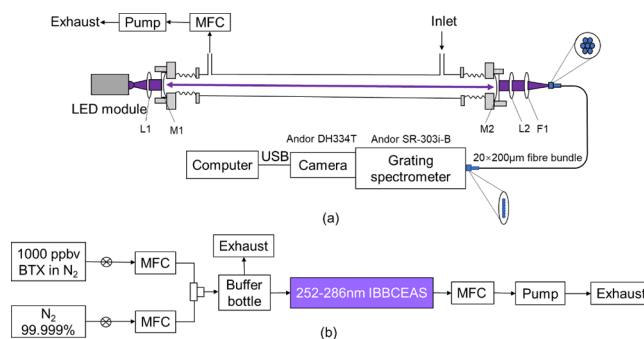


**Figure 1.** (a) A schematic of the DUV-IBBCEAS instrument for the measurement of benzene, toluene, and xylene. The optical portion of the instrument consists of a temperature-stabilized LED, collimating and focusing optics (lenses L1 and L2), a short-pass filter (F1), the optical cavity formed by plano-concave HR dielectric mirrors (M1 and M2), specialized fiber bundle, grating spectrometer, and a CCD detector. (b) Gas mixture and sampling system for generating different concentrations of benzene, toluene, and xylene. The sample gas is drawn through the cavity from the inlet using a diaphragm pump.

The detection module was a grating spectrograph (Andor SR-303i-B, Oxford Instruments) with a CCD detector (Andor DH334T-18 U-E3, Oxford instruments) cooled to  $-25.0 \text{ }^\circ\text{C}$  to minimize the dark current. The detector's Micro-Channel Plate (MCP) image intensifier can be varied to amplify the signal intensity. The spectrograph had a  $1200 \text{ L mm}^{-1}$  diffraction grating (300 nm blaze) and covered the range between 252 and 286 nm. The wavelength resolution was 0.74 nm, based on a fit to the 253.65 nm emission line of a commercial mercury lamp (Hg-1, Ocean Optics).

**2.2. Sample Handling.** Samples were introduced in a quartz flow tube (25 mm inner diameter) with a separation of 69.7 cm between the inlet and outlet (Figure 1b). The concentration of benzene, toluene, *m*-xylene, and *p*-xylene was generated by mixing a flow of N<sub>2</sub> (>99.999% purity) with the output of a gas cylinder comprising  $1.04 \pm 0.02 \text{ ppmv}$  for benzene,  $1.02 \pm 0.02 \text{ ppmv}$  for toluene,  $1.00 \pm 0.02 \text{ ppmv}$  for *m*-xylene, and  $1.02 \pm 0.02 \text{ ppmv}$  for *p*-xylene (Dalian Special Gases). Flow rates of the N<sub>2</sub> and aromatic gas mixture streams were controlled by mass flow controllers (MFC). The flow rates of BTX gases were controlled at 1000 sccm, and the N<sub>2</sub> flow rate was controlled at 666, 250, and 0 sccm, respectively. Thus, the BTX gas was diluted to 600, 800, and 1000 ppbv at about  $298 \pm 1 \text{ K}$  and  $101 \pm 1 \text{ kPa}$ . One hand of the cavity was connected to a buffer bottle, from which sample was drawn into the cavity at a flow rate of 800 sccm (controlled by an MFC) by a pump. Excess gas in the buffer bottle was discharged to the fume hood. MFC were calibrated by a flow meter (Gilibrator-2, Sensidyne).

**2.3. HR-Mirror Calibration.** In IBBCEAS systems, the extinction coefficient  $\epsilon_{\text{ext}}(\lambda)$  of the gas sample in the cavity is related to the measured properties and system parameters through the following relation:

$$\epsilon_{\text{ext}}(\lambda) = \left( \frac{I_0(\lambda)}{I(\lambda)} - 1 \right) \left( \frac{1 - R(\lambda)}{d} + \alpha_{\text{Rayl}}(\lambda) \right) \quad (1)$$

Here, instrument parameters are the cavity length  $d$ , the mirror reflectivity  $R(\lambda)$ , the measured reference and sample intensity spectra ( $I_0(\lambda)$  and  $I(\lambda)$ , respectively), and the extinction due to the Rayleigh scattering  $\alpha_{\text{Rayl}}(\lambda)$ . The mirror

reflectivity  $R(\lambda)$  is essential for quantitative results and must be calibrated. In previous work,  $R(\lambda)$  has been determined using different methods based on a known extinction in the cavity. There were also many other different calibration approaches.<sup>16,25–30</sup>

In this study, we used two approaches to determine the mirror reflectivity,  $R(\lambda)$ . The first approach used a known gas absorption of  $\text{SO}_2$  to determine the reflectivity,  $R_{\text{SO}_2}(\lambda)$ . A 1005 ppm  $\text{SO}_2$  gas mixture (in  $\text{N}_2$ ) was further diluted in a stream of pure nitrogen to 600 and 1000 ppbv with a multigas calibrator (164i, Thermal Fisher). The reflectivity  $R_{\text{SO}_2}(\lambda)$  can be determined from:

$$R_{\text{SO}_2}(\lambda) = 1 - d \left( \frac{\sigma_{\text{SO}_2}(\lambda) \cdot n_{\text{SO}_2}}{I_{\text{N}_2}(\lambda)/I_{\text{SO}_2}(\lambda) - 1} \right) \quad (2)$$

where  $I_{\text{N}_2}(\lambda)$  and  $I_{\text{SO}_2}(\lambda)$  are the measured light intensity when the cavity was filled with nitrogen and a known number density ( $n_{\text{SO}_2}$ ) of  $\text{SO}_2$ , respectively, and  $\sigma_{\text{SO}_2}(\lambda)$  is the literature absorption cross section of  $\text{SO}_2$ <sup>31</sup> convolved to our spectrograph instrument function. This approach gave an uncertainty in  $R_{\text{SO}_2}(\lambda)$  of about 4%, which is dominated by the uncertainty in the  $\text{SO}_2$  cross section.

The second approach used the difference in Rayleigh scattering of two pure gases for another determination of the mirror reflectivity,  $R_{\text{Rayl}}(\lambda)$ . Pure nitrogen (>99.999%) and pure helium (>99.999%) were used to determine  $R_{\text{Rayl}}(\lambda)$  according to eq 3:

$$R_{\text{Rayl}}(\lambda) = 1 - d \left( \frac{I_{\text{N}_2}(\lambda) \cdot n_{\text{N}_2} \cdot \sigma_{\text{Rayl,N}_2}(\lambda) - I_{\text{He}}(\lambda) \cdot n_{\text{He}} \cdot \sigma_{\text{Rayl,He}}(\lambda)}{I_{\text{He}}(\lambda) - I_{\text{N}_2}(\lambda)} \right) \quad (3)$$

where  $I_{\text{N}_2}(\lambda)$  and  $I_{\text{He}}(\lambda)$  represent the measured intensities when either nitrogen or helium, respectively, is in the cavity and  $\sigma_{\text{Rayl,N}_2}(\lambda)$  and  $\sigma_{\text{Rayl,He}}(\lambda)$  are the Rayleigh scattering cross sections of nitrogen and helium, respectively. The uncertainty of  $R_{\text{Rayl}}(\lambda)$  is about 5% and mainly determined by the uncertainty in the scattering cross section of  $\text{N}_2$  reported by Sneep and Ubachs.<sup>32</sup>

The intensity of the cavity at 1 s integration time is shown in Figure 2a. A wide spectral range from 250 to 295 nm can be achieved. As shown in Figure 2b, the reflectivity of the mirror exceeded 99.63% at its center near 266 nm. The averaged

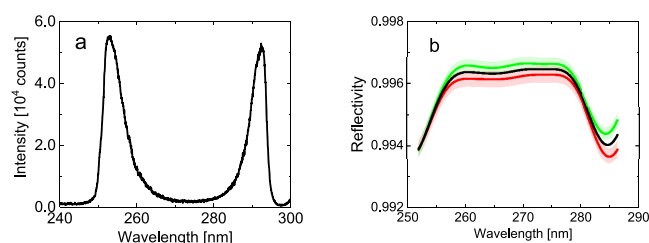


**Figure 2.** (a) The intensity of the cavity with 1800 gain at 1 s integration time. (b) Mirror reflectivities were calibrated with two methods: based on the difference in Rayleigh scattering of nitrogen and helium (green line) and based on a known  $\text{SO}_2$  absorption (red line) all with  $1\sigma$  precision. The black line represents the calculated mean mirror reflectivity from both methods.

reflectivity  $R(\lambda)$  was used in this instrument. Based on Gaussian error propagation, the uncertainty in  $R(\lambda)$  is 6.4%.

### 3. RESULTS AND DISCUSSION

**3.1. System Performance.** The optimal integration time for an instrument is commonly determined by calculating the Allan deviation:<sup>14,23,33–35</sup>

$$\sigma_{A_n}^2(t) = \frac{1}{2(M-2)} \sum_{i=1}^{M-2} [\alpha_{i+1}(t) - \alpha_i(t)]^2 \quad (4)$$

where  $t$  is the integration time,  $M$  is the number of time series, and  $\alpha_i(t)$  is the absorption coefficient in each subset from  $i = 1$  to  $i = M - 2$ . The Allan deviation  $\sigma_{A_n}(t)$  is the square root of  $\sigma_{A_n}^2(t)$ . A total of 20,000 reference spectra with 1 s exposure time were continuously measured over 5 h while the cavity was filled with pure nitrogen (>99.999%).

System sensitivity increased with integration time up to 1000 s (Figure 3). This result is not surprising because the system

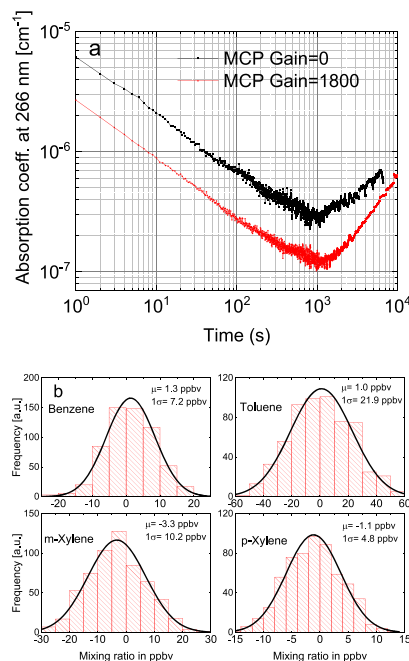


**Figure 3.** (a) Allan deviation of the absorption coefficient at 266 nm. For an integration time of 60 s and at a gain setting of 1800, the precision of the instrument is  $3.70 \times 10^{-7} \text{ cm}^{-1}$ . (b) The histogram analysis of the concentration measurement of benzene, toluene, *m*-xylene, and *p*-xylene based on 600 measurements of 60 s. Concentrations were retrieved by fitting the measured spectrum with the absorption cross sections convolved from Fally et al.<sup>36</sup>

precision was fundamentally limited by low light levels and longer averaging implies that more photons are measured. The system gain setting also influenced instrument precision for a given measurement time, with a higher gain producing better precision for a given integration time. The maximum precision of the instrument was  $2.3 \times 10^{-7} \text{ cm}^{-1}$  without the MCP image intensifier (Gain = 0); the precision improved to  $1.1 \times 10^{-7} \text{ cm}^{-1}$  using the MCP image intensifier with Gain = 1800. The retrieval precision of the DUV-IBBCEAS system to BTX over a 60 s acquisition time was estimated by fitting the zero air spectrum to the BTX absorption cross sections reported by Fally et al.<sup>36</sup> A histogram analysis of 600 zero measurements is

shown in Figure 3b. The  $1\sigma$  measurement precision was 7.2 ppbv for benzene, 21.9 ppbv for toluene, 10.2 ppbv for *m*-xylene, and 4.8 ppbv for *p*-xylene, respectively.

**3.2. Absorption Cross-Section Measurement.** Table 1 summarizes previous determinations of gas-phase absorption

**Table 1. Instrumental Parameters of Literature Absorption Cross Sections**

references	temp. (K)	pressure (mbar)	wavelength (nm)	resolution (nm)
Benzene				
Trost et al. (1997) <sup>38</sup>	293.5	1000	230–278	0.11
Etzkorn et al. (1999) <sup>39</sup>	298	1000	235–276	0.15
Fally et al. (2009) <sup>36</sup>	293	1.33	239–270	0.007
Olive (2015) <sup>40</sup>	298	N.A.	200–265	0.13
Dawes et al. (2017) <sup>37</sup>	298	10 <sup>-9</sup>	115–330	0.1
Toluene				
Etzkorn et al. (1999) <sup>39</sup>	298	1000	237–278	0.15
Koban et al. (2004) <sup>41</sup>	296	1000	227–273	1
Olive (2005) <sup>40</sup>	298	N.A.	225–285	0.08
Fally et al. (2009) <sup>36</sup>	293	3.05	242–278	0.007
<i>m</i> -Xylene				
Bolovinos et al. (1982) <sup>42</sup>	298	33.3	139–280	0.25
Trost et al. (1997) <sup>38</sup>	293.5	1000	239–278	0.11
Etzkorn et al. (1999) <sup>39</sup>	298	1000	242–283	0.15
Olive (2005) <sup>40</sup>	298	N.A.	235–285	0.05
Fally et al. (2009) <sup>36</sup>	293	4.12	242–286	0.007
<i>p</i> -Xylene				
Bolovinos et al. (1982) <sup>42</sup>	298	33.3	139–280	0.25
Trost et al. (1997) <sup>38</sup>	293	1000	239–278	0.11
Etzkorn et al. (1999) <sup>39</sup>	298	1000	242–283	0.15
Olive (2005) <sup>40</sup>	298	N.A.	235–285	0.05
Fally et al. (2009) <sup>36</sup>	293	2.08	242–286	0.007

cross sections of benzene, toluene, *m*-xylene, and *p*-xylene at room temperature and at different pressures and resolutions.

**3.2.1. Benzene.** The absorption coefficients were measured over a 30 min integration time. The absorption coefficients of benzene at 600, 800, and 1000 ppbv obtained in this work are shown in Figure S1(a). Figure 4a shows that the absorption

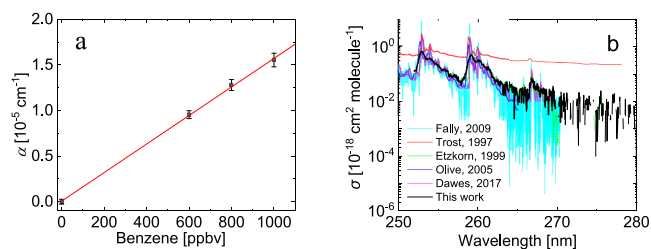


**Figure 4.** (a) Dependence of the benzene absorption coefficient at 252.96 nm on concentration. The correlation coefficient of the linear regression is  $R^2 > 0.999$ . (b) Benzene absorption cross section from this work and recent literature spectrum.<sup>36–40</sup> Note that the *y*-axis uses a logarithmic scale.

coefficient at 253 nm is linearly correlated with concentration ( $R^2 > 0.999$ ). The intercept ( $6.88 \times 10^{-8} \text{ cm}^{-1}$ ) and its standard deviation ( $1.95 \times 10^{-7} \text{ cm}^{-1}$ ) are both small.

The UV absorption of benzene is attributed to the  $S_1(^1B_{2u}) \leftarrow S_0(^1A_{1g})$  electronic transition.<sup>36</sup> Narrow vibrational transitions dominate in this range, and spectral resolution strongly affects the measured spectrum. The absorption cross

section of benzene measured in this work is compared against prior work in Figure 4b. Two major absorption peaks are apparent in our measurement window. The position of the absorption peaks reported in our study is consistent with the data of Fally et al.<sup>36</sup> and Dawes et al.,<sup>37</sup> whereas the spectrum reported by Olive<sup>40</sup> is shifted  $-0.2 \text{ nm}$  compared to others. For highly structured spectral features, the instrument resolution has a large effect, and high-intensity structures are apparent in the high-resolution measurements of Fally et al.<sup>36</sup> These features are smoothed out at coarser resolution. Indeed, the resolution of our instrument is a factor of 4 or more lower than other measurements. The absorption cross section of recent literature convolved to this work's resolution is shown in Figure S2.

The absorption cross-sections reported in this work were the mean value obtained by averaging the absorption cross-sections of three concentrations (600, 800, and 1000 ppbv) and were in good agreement with cross sections obtained by linear regression analysis.

**3.2.2. Toluene.** The absorption coefficients of toluene at 600, 800, and 1000 ppbv obtained in this work are shown in Figure S1(b). As with benzene, the absorption (at 267 nm) was highly linear ( $R^2 > 0.999$ ) with toluene concentration (Figure 5a), and the intercept was small  $4.65 \times 10^{-8} \text{ cm}^{-1}$  (standard deviation of  $8.22 \times 10^{-8} \text{ cm}^{-1}$ ).

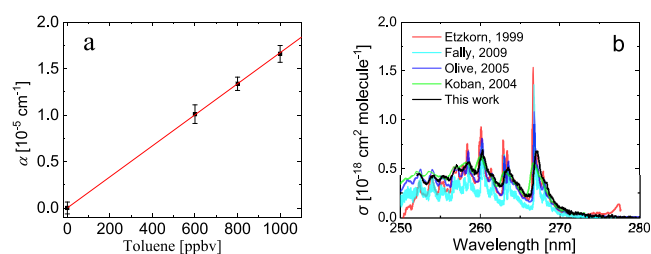


**Figure 5.** (a) Dependence of the toluene absorption coefficient on the different concentrations at 267 nm. The correlation coefficient of the linear regression is  $R^2 \geq 0.999$ . (b) Toluene absorption cross-section from this work and recent literature spectrum.<sup>36,39–41</sup> Note that the *y*-axis scale is linear.

Figure 5b shows the absorption cross section of toluene measured with the DUV-IBBCEAS system, together with the cross sections of Etzkorn et al.,<sup>39</sup> Koban et al.,<sup>41</sup> Olive,<sup>40</sup> and Fally et al.<sup>36</sup> The agreement between our cross section and those of Etzkorn et al.,<sup>39</sup> Koban et al.,<sup>41</sup> and Olive<sup>40</sup> is generally good, while the cross section reported by Fally et al.<sup>36</sup> is lower than other studies.

**3.2.3. *m*-Xylene.** The absorption coefficients of *m*-xylene at 600, 800, and 1000 ppbv obtained in this work are shown in Figure S1(c). The three absorption coefficients at 271 nm are compared in Figure 6a and also highly linear with concentration ( $R^2 > 0.999$ ) with a small *y*-intercept  $5.78 \times 10^{-8} \text{ cm}^{-1}$  (standard deviation of  $1.55 \times 10^{-7} \text{ cm}^{-1}$ ).

The absorption cross section of *m*-xylene measured in this work is shown in Figure 6b, together with the spectra of Bolovinos et al.,<sup>42</sup> Trost et al.,<sup>38</sup> Etzkorn et al.,<sup>39</sup> Olive,<sup>40</sup> and Fally et al.<sup>36</sup> The agreement between the absorption cross section measured in this work, and those reported previously are good, with the notable exception of the cross section reported by Trost et al.,<sup>38</sup> which had a relatively large positive offset (see also Figure 4b for comparison with the work of Trost et al.).

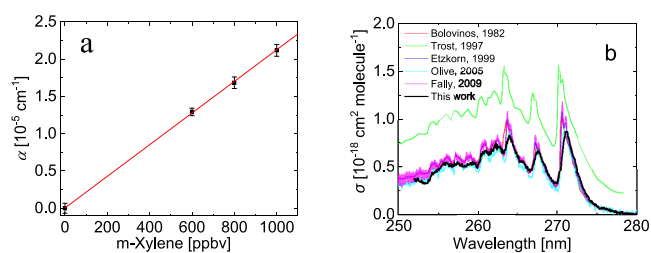


**Figure 6.** (a) Dependence of the *m*-xylene absorption coefficient on the different concentrations at 271 nm. The correlation coefficient of the linear regression is  $R^2 > 0.999$ . (b) *m*-Xylene absorption cross section from this work and recent literature spectrum.<sup>36,38–40,42</sup>

**3.2.4. *p*-Xylene.** The absorption coefficients of *p*-xylene at 600, 800, and 1000 ppbv obtained in this work are shown in Figure S1(d), and the three absorption coefficients at 273 nm are compared in Figure 7a. The absorption was linear with concentration ( $R^2 > 0.999$ ) with a small  $y$ -intercept  $1.82 \times 10^{-7} \text{ cm}^{-1}$  with a standard deviation of  $4.17 \times 10^{-7} \text{ cm}^{-1}$ .

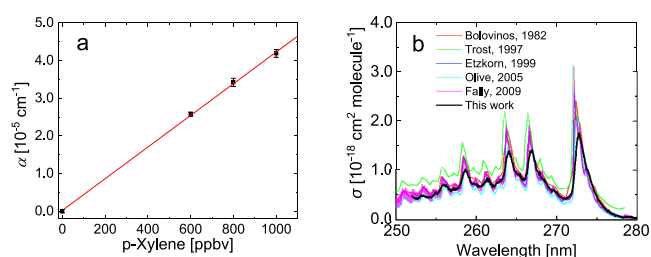


**Figure 7.** (a) Dependence of the *p*-xylene absorption coefficient on the different concentrations at 272.79 nm. The correlation coefficient of the linear regression is  $R^2 > 0.999$ . (b) *p*-Xylene absorption cross section from this work and recent literature spectrum.<sup>36,38–40,42</sup>

The absorption cross section of *p*-xylene measured in this work is shown in Figure 7b, together with the spectra of Bolovinos et al.,<sup>42</sup> Trost et al.,<sup>38</sup> Etzkorn et al.,<sup>39</sup> Olive,<sup>40</sup> and Fally et al.<sup>36</sup> The agreement between the spectrum in this work, and the spectra reported by literature are good over this region. The spectrum reported by Trost et al.<sup>38</sup> was marginally higher than other values.

**3.2.5. Uncertainty of Cross Section.** The uncertainty in our absorption cross-section measurements was estimated using standard uncertainty propagation. The uncertainty of extinction coefficient  $\epsilon$ , can be calculated by eq 5:<sup>16</sup>

$$\begin{aligned} \Delta \epsilon^2 &= \left| \frac{\partial \epsilon}{\partial d} \right|^2 \cdot \Delta d^2 + \left| \frac{\partial \epsilon}{\partial (1-R)} \right|^2 \cdot \Delta (1-R)^2 + \left| \frac{\partial \epsilon}{\partial I_0} \right|^2 \cdot \Delta I_0^2 \\ &= \epsilon^2 \left( \frac{\Delta d}{d} \right)^2 + \epsilon^2 \left( \frac{\Delta (1-R)}{1-R} \right)^2 + \left( \frac{1-R}{d} \right)^2 \cdot \left( \frac{\Delta I_0}{I} \right)^2 \end{aligned} \quad (5)$$

where  $\Delta d$ ,  $\Delta(1-R)$ , and  $\Delta I_0$  are the uncertainties in the cavity length, mirror reflectivity, and spectral intensity, respectively. The relative uncertainties in eq 6 are 1% for  $d$ , 6.4% for  $1-R$  (according to the uncertainty of  $R$ ), and 3.5% for intensity fluctuations at a 1 min integration time. The overall uncertainty in the extinction measurement is therefore around 9.8% and is dominated by the uncertainty in the mirror reflectivity.

The uncertainty in the absorption cross section must also account for the uncertainty in the concentration of each species ( $\Delta N$ ):

$$\left( \frac{\Delta \sigma}{\sigma} \right)^2 = \left( \frac{\Delta \epsilon}{\epsilon} \right)^2 + \left( \frac{\Delta N}{N} \right)^2 \quad (6)$$

The uncertainties in the concentrations of gas cylinder are 2% for benzene, toluene, *m*-xylene, and *p*-xylene according to the manufacturer. The uncertainty in flowrate is 0.35% F.S. according to the manufacturer and calibrated by a flow meter (Gilibrator-2, Sensidyne). And the combined uncertainty in absorption cross sections is thus 10.0% for all four gases at a resolution of 0.74 nm.

**3.3. Measurement of Xylene Isomers.** The least-squares spectral fitting method was used to demonstrate that deep-UV spectral analysis could be used to quantify the concentrations of different xylene isomers at the same time. The optimized spectral fitting window was from 258 to 278 nm. A third-order polynomial was applied to fit the shape of the background spectrum, which was mainly produced by the spectral dependence of the mirror reflectivity and from sample scattering. The reported absorption cross sections of xylene in this work were used to retrieve the concentration of xylene isomers. As shown in Figure 8a, five sets of *m*-xylene/*p*-xylene

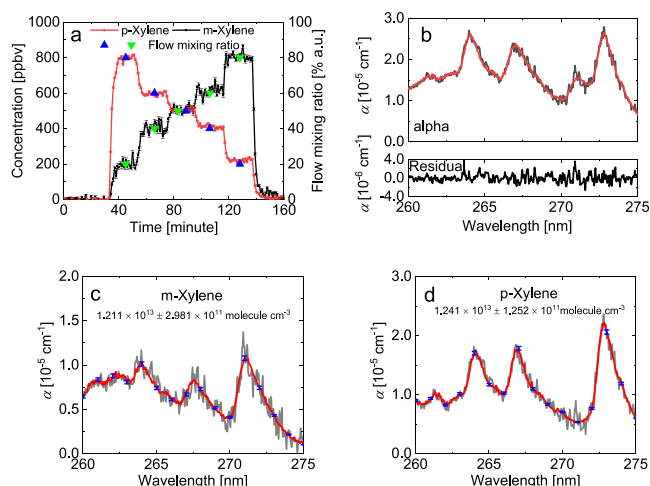


**Figure 8.** (a) Measurement result of five different concentrations of *p*-xylene (red line and circle) and *m*-xylene (black lines and squares) standard gases. The blue positive triangle and green inverted triangle represent the flow ratios of the *p*-xylene and *m*-xylene standard gas mixtures, respectively. (b) An example spectral fit to one spectrum measured 83 min from the start of the experiment. The retrieved spectral fits of *m*-xylene (c) and *p*-xylene (d). The red line represents the fitted spectrum, and the black line is the fitted result plus the residual with  $1\sigma$  error bar.

mixtures diluted by standard gas cylinders were measured with an integration time of 60 s. During the experiment, the fractional flowrate of *p*-xylene was reduced in a stepwise manner (80, 60, 50, 40, and 20%); the fractional flow rate of *m*-xylene was increased sequentially from 20, 40, 50, 60, and 80%. The uncertainty of retrieved concentration was dominated by absorption cross section and reflectivity.

Figure 8b,c,d shows an example of the spectral fitting of a spectrum of the *m*-xylene and *p*-xylene mixture measured 83 min from the start of the experiment. The retrieved mixing ratios of *m*-xylene and *p*-xylene were  $493 \pm 12$  ppbv and  $505 \pm$

5 ppbv, respectively. The corresponding fitting residual is in the range of  $\pm 7.6 \times 10^{-7} \text{ cm}^{-1}$ .

**3.4. Discussion.** The instrument presented in this work represents an important advance in the application of broadband optical cavity techniques to deep-UV wavelengths. We applied our system to quantify the important anthropogenic environmental pollutants BTX. Nevertheless, we emphasize that the method has general application to other compounds that absorb in this region, as well as to particle extinction measurements. This work therefore has broad applicability to a range of applications and research fields, whether for air quality or emissions monitoring, pure or applied laboratory research, or other technological applications. In the following, we discuss considerations around the BTX measurements presented in this work, propose instrumental improvements and measurement strategies, and assess their use in different applications.

The  $1\sigma$  measurement precisions of the DUV-IBBCEAS system over a 60 s acquisition time (7.2 ppbv ( $1\sigma$ ) for benzene, 21.9 ppbv ( $1\sigma$ ) for toluene, 10.2 ppbv ( $1\sigma$ ) for *m*-xylene and 4.8 ppbv ( $1\sigma$ ) for *p*-xylene) are already sufficient to be relevant to a range of applications, including fence-line and continuous emissions monitoring of these species. It also provides a potentially useful tool for analytical chemistry in combination with pre-concentration or chromatographic approaches. These ideas will be explored in future work to monitor atmospheric BTX.

Several strategies are possible to further improve the system sensitivity. Our spectrometer used a relatively low-resolution configuration to increase light throughput owing to the challenges of working with low light levels in the deep UV. Although there is a trade-off between resolution and optical throughput, higher resolution spectra would be advantageous for capturing highly structured spectral features (for benzene, in particular) with improved sensitivity and selectivity.

Light source intensity is a major technical challenge in this spectral region. The advantages of deep-UV LEDs are that they are relatively inexpensive light sources, produce stable emission intensities with careful control of temperature and current and do not need extensive spectral filtering. Other light sources with deep-UV output could prove advantageous for some applications. LDLS or Xe flashlamps have relatively high-intensity DUV output and could be useful alternative sources but would require stringent filtering to remove unwanted wavelengths from the optical system. Deuterium lamps would be challenging to use at these wavelengths because they are not particularly bright.

For applications where lower absorption sensitivities would suffice, light throughput could be raised by using lower reflectivity mirrors in the optical cavity, resulting in greater throughput and higher time resolution, at the cost of a shorter effective light path length and lower sensitivity.

In addition to the technological challenges described above, absorption by ozone is also at its maximum in this spectral region and could prove challenging for working with ambient air samples. Appreciable absorption by  $\text{O}_3$  in a sample would reduce the overall instrument sensitivity. An  $\text{O}_3$  denuder in the inlet line could circumvent this issue, albeit at the cost of greater system complexity. Alternatively, sample preconcentration could be used to attain much higher sensitivities and avoid some interferences while retaining almost real-time measurement capability. We will explore the application of the DUV-

IBBCEAS system to the measurement of ozone concentrations in future work.

The influence of other atmospheric constituents on system performance should also be considered. The common atmospheric pollutant  $\text{NO}_2$  has an absorption cross section between 250 and 280 nm that is around two orders of magnitude lower than ozone and BTX species. Unless present in much higher concentrations than BTX, the influence of  $\text{NO}_2$  absorption on the retrieval of BTX concentration will be negligible. However, aerosol extinction, mainly from Mie scattering, can exceed  $10^{-6} \text{ cm}^{-1}$  in a polluted environment.<sup>27,43</sup> Such high extinctions will substantially reduce the effective path length of light in the cavity and hence lower the instrument sensitivity. In our instrument, for instance, the effective path length at 266 nm is ca. 189 m under minimal aerosol conditions but decreases to below 160 m when the aerosol extinction coefficient is  $10^{-6} \text{ cm}^{-1}$ . To minimize the effect of ambient aerosols, a simple solution is to install a particle filter in the inlet stream.

This work shows the potential of the IBBCEAS approach for measurements of absorbing gases in the deep UV. Many other volatile species absorb between 250 and 280 nm, notably carbonyl species and other small aromatics,  $\text{SO}_2$  (as used to calibrate our instrument), organic reaction intermediates and radicals (like the ethyl, benzyl, and phenyl radicals, the phenoxy radical, and the phenyl, methyl, and benzyl peroxy radicals), and a range of chlorine oxide species ( $\text{ClO}$ ,  $\text{ClOO}$ ,  $\text{ClOOCl}$ ,  $\text{Cl}_2\text{O}$ ,  $\text{Cl}_2\text{O}_6$ ). For research applications, spectroscopic methods would have exceptional sensitivity to these highly unstable species and the ability to measure them in situ would be valuable tools.

It is also worth pointing out that the 200–230 nm spectral region is particularly important for the measurement of the key environmental gases  $\text{NH}_3$ ,  $\text{SO}_2$ , isoprene, and  $\text{NO}$ , even if commercially available DUV LEDs cannot yet attain such short wavelengths, and mirror reflectivities are worse at these short wavelengths. Some active DOAS systems have already demonstrated high sensitivity in this region with light paths of 100 m,<sup>44</sup> which is useful for sampling particularly sticky gases like  $\text{NH}_3$ .

## 4. CONCLUSIONS

This study presented a novel IBBCEAS system for the measurement of BTX. Combined with the 255 nm LED, optical cavity, and short-pass filter, a spectral range from 250 to 295 nm was achieved. The absorption cross sections of benzene, toluene, *p*- and *m*-xylene measured with the spectrometer were in good agreement with previous work by others. We demonstrated the application of the system to the simultaneous retrieval of mixtures of *m*-xylene and *p*-xylene. The extension of the approach to other species of scientific and technological interest, as well as ways to optimize the spectrometer for different purposes, was discussed.

## ■ ASSOCIATED CONTENT

### Supporting Information

The Supporting Information is available free of charge at <https://pubs.acs.org/doi/10.1021/acs.analchem.1c04940>.

Figure S1, the absorption coefficient of BTX; Figure S2, the absorption cross section of benzene (PDF)

## AUTHOR INFORMATION

## Corresponding Author

**Jun Chen** – Shanghai Key Laboratory of Multiphase Flow and Heat Transfer in Power Engineering, School of Energy and Power Engineering, University of Shanghai for Science and Technology, Shanghai 200093, China; [orcid.org/0000-0002-0334-6846](https://orcid.org/0000-0002-0334-6846); Email: [j.chen@usst.edu.cn](mailto:j.chen@usst.edu.cn)

## Authors

**Meng Wang** – Shanghai Key Laboratory of Multiphase Flow and Heat Transfer in Power Engineering, School of Energy and Power Engineering, University of Shanghai for Science and Technology, Shanghai 200093, China

**Ravi Varma** – Department of Physics, National Institute of Technology Calicut, Calicut, Kerala 673601, India; [orcid.org/0000-0003-4628-3651](https://orcid.org/0000-0003-4628-3651)

**Dean S. Venables** – School of Chemistry and Environmental Research Institute, University College Cork, Cork T12 K8AF, Ireland

**Wu Zhou** – Shanghai Key Laboratory of Multiphase Flow and Heat Transfer in Power Engineering, School of Energy and Power Engineering, University of Shanghai for Science and Technology, Shanghai 200093, China

Complete contact information is available at:  
<https://pubs.acs.org/10.1021/acs.analchem.1c04940>

## Author Contributions

M.W. was in charge of investigation, data curation, formal analysis, validation, and writing the original draft. R.V. was in charge of conceptualization and investigation. D.V. performed the conceptualization, methodology, writing, review as well as editing. W.Z. performed the conceptualization and funding acquisition. J.C. was in charge of conceptualization, methodology, investigation, supervision, funding acquisition, writing, review, and editing.

## Funding

This work was supported by the National Natural Science Foundation of China (Grant Nos. 91544225, 51776129), the National Key Research and Development Program of China (Grant Nos. 2017YFC0211504 and 2018YFC0213800).

## Notes

The authors declare no competing financial interest.

## REFERENCES

- (1) Pereira, K. L.; Hamilton, J. F.; Rickard, A. R.; Bloss, W. J.; Alam, M. S.; Camredon, M.; Ward, M. W.; Wyche, K. P.; Munoz, A.; Vera, T.; Vazquez, M.; Borrás, E.; Rodenas, M. *Environ. Sci. Technol.* **2015**, *49*, 13168–13178.
- (2) Lee, S. C.; Chiu, M. Y.; Ho, K. F.; Zou, S. C.; Wang, X. M. *Chemosphere* **2002**, *48*, 375–382.
- (3) Liu, J.; Li, X.; Yang, Y.; Wang, H.; Wu, Y.; Lu, X.; Chen, M.; Hu, J.; Fan, X.; Zeng, L.; Zhang, Y. *Atmos. Meas. Tech.* **2019**, *12*, 4439–4453.
- (4) Thalman, R.; Volkamer, R. *Atmos. Meas. Tech.* **2010**, *3*, 1797–1814.
- (5) Washenfelder, R. A.; Langford, A. O.; Fuchs, H.; Brown, S. S. *Atmos. Chem. Phys.* **2008**, *8*, 7779–7793.
- (6) Qi, X.; Zhu, S.; Zhu, C.; Hu, J.; Lou, S.; Xu, L.; Dong, J.; Cheng, P. *Sci. Total Environ.* **2020**, *727*, No. 138632.
- (7) Wang, H.; Gao, Y.; Wang, S.; Wu, X.; Liu, Y.; Li, X.; Huang, D.; Lou, S.; Wu, Z.; Guo, S.; Jing, S.; Li, Y.; Huang, C.; Tyndall, G. S.; Orlando, J. J.; Zhang, X. *J. Geophys. Res.: Atmos.* **2020**, *125*, No. e2020JD033401.
- (8) Yuan, B.; Koss, A. R.; Warneke, C.; Coggon, M.; Sekimoto, K.; de Gouw, J. A. *Chem. Rev.* **2017**, *117*, 13187–13229.
- (9) Noziere, B.; Kaberer, M.; Claeys, M.; Allan, J.; D'Anna, B.; Decesari, S.; Finessi, E.; Glasius, M.; Grgic, I.; Hamilton, J. F.; Hoffmann, T.; Iinuma, Y.; Jaoui, M.; Kahno, A.; Kampf, C. J.; Kourtchev, I.; Maenhaut, W.; Marsden, N.; Saarikoski, S.; Schnelle-Kreis, J.; Surratt, J. D.; Szidat, S.; Szmigielski, R.; Wisthaler, A. *Chem. Rev.* **2015**, *115*, 3919–3983.
- (10) Stutz, J.; Hurlock, S. C.; Colosimo, S. F.; Tsai, C.; Cheung, R.; Festa, J.; Pikel'naya, O.; Alvarez, S.; Flynn, J. H.; Erickson, M. H.; Olaguer, E. P. *Atmos. Environ.* **2016**, *147*, 121–132.
- (11) Isac, B. *Differential optical absorption spectroscopy (DOAS)*, 1994.
- (12) Fiedler, S. E.; Hese, A.; Ruth, A. A. *Chem. Phys. Lett.* **2003**, *371*, 284–294.
- (13) Titus, G.; Venables, D. S.; Stewart, V.; Johannes, O.; Ruth, A. A. *Environ. Sci. Technol.* **2008**, *42*, 890–895.
- (14) Liu, J.; Li, X.; Yang, Y.; Wang, H.; Kuang, C.; Zhu, Y.; Chen, M.; Hu, J.; Zeng, L.; Zhang, Y. *Anal. Chem.* **2020**, *92*, 2697–2705.
- (15) Jordan, N.; Osthoff, H. D. *Atmos. Meas. Tech.* **2020**, *13*, 273–285.
- (16) Chen, J.; Venables, D. S. *Atmos. Meas. Tech.* **2011**, *4*, 425–436.
- (17) Chen, J.; Wenger, J. C.; Venables, D. S. *J. Phys. Chem. A* **2011**, *115*, 12235–12242.
- (18) Ityaksov, D.; Linnartz, H.; Ubachs, W. *Mol. Phys.* **2008**, *106*, 2471–2479.
- (19) Darby, S. B.; Smith, P. D.; Venables, D. S. *Analyst* **2012**, *137*, 2318–2321.
- (20) Islam, M.; Ciaffoni, L.; Hancock, G.; Ritchie, G. A. *Analyst* **2013**, *138*, 4741–4745.
- (21) Aoyagi, Y.; Takeuchi, M.; Yoshida, K.; Kurouchi, M.; Araki, T.; Nanishi, Y.; Sugano, H.; Ahiko, Y.; Nakamura, H. *J. Environ. Prot.* **2012**, *03*, 695–699.
- (22) Li, C. M.; Wang, H. C.; Chen, X. R.; Zhai, T. Y.; Chen, S. Y.; Li, X.; Zeng, L. M.; Lu, K. D. *Atmos. Meas. Tech.* **2021**, *14*, 4033–4051.
- (23) Wang, H.; Chen, J.; Lu, K. *Atmos. Meas. Tech.* **2017**, *10*, 1465–1479.
- (24) Ball, S. M.; Langridge, J. M.; Jones, R. L. *Chem. Phys. Lett.* **2004**, *398*, 68–74.
- (25) Venables, D. S.; Titus, G.; Johannes, O.; Wenger, J. C.; Ruth, A. A. *Environ. Sci. Technol.* **2006**, *40*, 6758.
- (26) Washenfelder, R. A.; Attwood, A. R.; Flores, J. M.; Zarzana, K. J.; Rudich, Y.; Brown, S. S. *Atmos. Meas. Tech.* **2016**, *9*, 41–52.
- (27) Varma, R. M.; Venables, D. S.; Ruth, A. A.; Heitmann, U.; Schlosser, E.; Dixneuf, S. *Appl. Opt.* **2009**, *48*, B159–B171.
- (28) Fullam, D. P.; Shoji, K.; Venables, D. S. *Anal. Methods* **2015**, *7*, 3298–3301.
- (29) Schuster, G.; Labazan, I.; Crowley, J. N. *Atmos. Meas. Tech.* **2009**, *2*, 1–13.
- (30) Schmidl, G.; Paa, W.; Triebel, W.; Schippel, S.; Heyer, H. *Appl. Opt.* **2009**, *48*, 6754–6759.
- (31) Vandaele, A. C.; Hermans, C.; Fally, S. *J. Quant. Spectrosc. Radiat. Transfer* **2009**, *110*, 2115–2126.
- (32) Sneep, M.; Ubachs, W. *J. Quant. Spectrosc. Radiat. Transfer* **2005**, *92*, 293–310.
- (33) Allan, D. W. *Proc. IEEE* **1966**, *54*, 221–230.
- (34) Langridge, J. M.; Ball, S. M.; Shillings, A. J. L.; Jones, R. L. *Rev. Sci. Instrum.* **2008**, *79*, No. 123110.
- (35) Wu, T.; Chen, W.; Fertein, E.; Cazier, F.; Dewaele, D.; Gao, X. *Appl. Phys. B: Lasers Opt.* **2012**, *106*, 501–509.
- (36) Fally, S.; Carleer, M.; Vandaele, A. C. *J. Quant. Spectrosc. Radiat. Transfer* **2009**, *110*, 766–782.
- (37) Dawes, A.; Pascual, N.; Hoffmann, S. V.; Jones, N. C.; Mason, N. J. *Phys. Chem. Chem. Phys.* **2017**, *19*, 27544–27555.
- (38) Trost, B.; Stutz, J.; Platt, U. *Atmos. Environ.* **1997**, *31*, 3999–4008.
- (39) Eitzkorn, T.; Klotz, B.; Sorensen, S.; Patroescu, I. V.; Barnes, I.; Becker, K. H.; Platt, U. *Atmos. Environ.* **1999**, *33*, 525–540.

(40) The results reported by Olive were obtained from the MPI-Mainz UV/VIS Spectral Atlas of Gaseous Molecules of Atmospheric Interest. See: Keller-Rudek, H.; Moortgat, G.; Sander, R.; Sørensen, R. *Earth Syst. Sci. Data* **2013**, *5*, 365–373 ([http://satellite.mpic.de/spectral\\_atlas](http://satellite.mpic.de/spectral_atlas)).

(41) Koban, W.; Koch, J. D.; Hanson, R. K.; Schulz, C. *Phys. Chem. Chem. Phys.* **2004**, *6*, 2940.

(42) Bolovinos, A.; Philis, J.; Pantos, E.; Tsekeris, P.; Andritsopoulos, G. *J. Mol. Spectrosc.* **1982**, *94*, 55–68.

(43) John, S.; Wang, M.; Chen, J.; Pakkatil, A.; Du, Y.; Zhang, J.; Ramachandran, A.; Saseendran, A.; Thomas, A. P.; Viswanathan, D.; Mazzoleni, C.; Varma, R. *Aerosol Sci. Technol.* **2021**, *55*, 1264–1276.

(44) Volten, H.; Bergwerff, J. B.; Haaima, M.; Lolkema, D. E.; Berkhout, A. J. C.; van der Hoff, G. R.; Potma, C. J. M.; Wichink Kruit, R. J.; van Pul, W. A. J.; Swart, D. P. J. *Atmos. Meas. Tech.* **2012**, *5*, 413–427.